Sci. Bull. (2015) 60(19):1698–1707
DOI 10.1007/s11434-015-0890-0

www.scibull.com
www.springer.com/scp

Article

Earth Sciences

Metamorphism and zircon U–Pb dating of garnet amphibolite in the Baoyintu Group, Inner Mongolia

Yaping Chen · Chunjing Wei · Jinrui Zhang · Hang Chu

Received: 8 August 2015 / Accepted: 26 August 2015 / Published online: 24 September 2015

Abstract Garnet amphibolite in the Baoyintu Group, Inner Mongolia, is mainly composed of garnet, hornblende, plagioclase, quartz and minor rutile/ilmenite. Garnet occurs as porphyroblasts surrounded by plagioclase, forming typical "white-eye socket" texture. Garnet shows grossular content of 0.26–0.28 and pyrope of 0.11–0.13, without significant zoning. Plagioclase is generally zoned with anorthite (An) increasing from core to rim. The *P–T* pseudosection calculated using THERMOCALC in the system MnNCKFMASHTO shows that the garnet amphibolite experienced a clockwise *P–T* path with a peak at ~1.3 GPa/725 °C defined from the minimum An content in plagioclase and maximum pyrope content in garnet, followed by an isothermal decompression. LA-ICP-MS zircon dating for the garnet amphibolite indicates metamorphic ages of 399 ± 6 Ma. The peak *P–T* condition corresponds to a thermal gradient of ~18 °C/km, indicating typical medium-pressure type that commonly occurs in orogenic process with crustal thickening. We prefer to interpret this orogenic event to be a result of collision, following the closure of the Paleo-Asian Ocean before the early Devonian although there is a popular view that the Paleo-Asian Ocean may have lasted to the early Mesozoic.

Keywords Amphibolite · *P–T* pseudosection · Zircon U–Pb dating · Baoyintu Group · Central Asian Orogenic Belt

1 Introduction

The Central Asian Orogenic Belt (CAOB) is a giant accretionary orogen among the Siberian Craton, the North China Craton (NCC) and Tarim Craton, which is characterized by a series of island arcs, forearc or backarc basins, ophiolitic belts and microcontinents from the Neoproterozoic to Mesozoic [1, 2]. The tectonic evolution of CAOB has been highly disputed. Some geologists propose that the Paleo-Asian Ocean was ultimately closed in Late Permian–Early Mesozoic [2–6], but others emphasize the closure of the Paleo-Asian Ocean happened in Devonian which was followed by an extensional tectonic environment in the late Paleozoic [7–15]. In general, a collision-related orogeny resulted from an ocean closure may cause medium-pressure or kyanite-type metamorphism [16, 17]. However, the metamorphism related to the tectonic evolution of the Paleo-Asian Ocean has been rarely investigated. The Baoyintu Group is located in an area which was controversially considered as the basement of the CAOB [18–20] or the northern part of NCC [21] (Fig. 1a). It develops typical medium-pressure progressive garnet, staurolite and kyanite zones with numerous garnet amphibolite blocks or lenses [18]; however, its metamorphic *P–T* paths, metamorphic ages and related tectonic settings are not well constrained. The paper is aimed to reveal the metamorphic *P–T* conditions, paths and ages through investigating garnet amphibolite in the Baoyintu Group to constrain the tectonic evolution of CAOB.

Electronic supplementary material The online version of this article (doi:10.1007/s11434-015-0890-0) contains supplementary material, which is available to authorized users.

Y. Chen · C. Wei (✉) · J. Zhang
Key Laboratory of the Orogenic Belt and Crustal Evolution, Ministry of Education, School of Earth and Space Sciences, Peking University, Beijing 100871, China
e-mail: cjwei@pku.edu.cn

H. Chu
Tianjing Institute of Geology and Mineral Resources, Tianjin 300170, China

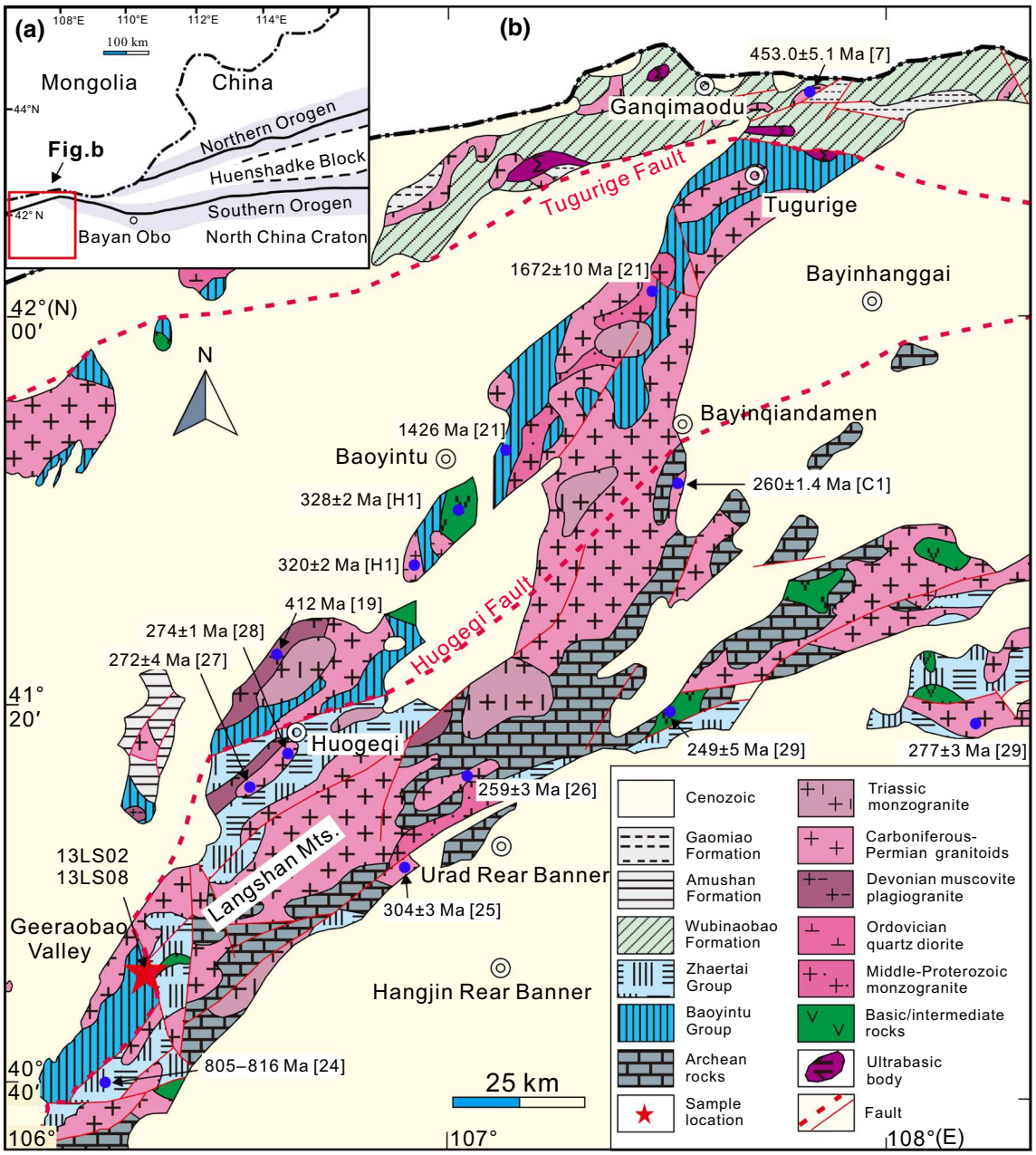

Fig. 1 (Color online) **a** Geological map of Inner Mongolia showing the tectonic framework of the study area [7]. **b** Detail geological map of central west Inner Mongolia showing the distribution of Baoyintu Group and sample locality [19]. The isotopic ages are cited from literatures with the reference numbers where H1 and C1 are the unpublished data from B. Han and H. Chu through personal communication

2 Geological setting

The Baoyintu Group is mainly distributed in Huogeqi, Baoyintu and Tugurige areas, the middle west Inner Mongolia (Fig. 1b). It is comprised of (garnet) amphibolites, (garnet, kyanite, staurolite) mica schists, quartzites and marbles. This metamorphic sequence was divided to the Inner Mongolia prairie stratigraphic region and proposed to be formed in Paleo-Proterozoic, forming the basement of CAOB [19]. This was supported by a Sm–Nd whole-rock isochron of 2,485 ± 128 Ma from amphibolite of the Baoyintu Group at Tugurige [20]. However, Sun et al. [21] obtained a low-limit detrital zircon U–Pb age of 1,426 Ma, and an age spectrum that is almost the same as that of the NCC from a quartzite of the Baoyintu Group, thus, proposed that the Baoyintu Group should be a part of

the NCC, presenting a rift setting in the passive continental margin of the craton.

Closely related to the Baoyintu Group in the Langshan Mts., the Zhaertai Group is composed of a regressive sequence involving clastic rocks, carbonates and basic and intermediate-acidic volcanic rocks metamorphosed under greenschist facies, which was considered to be the earliest cover of the Proterozoic in the northwest margin of the NCC northwest margin [22, 23]. Peng et al. [24] obtained an zircon U–Pb age of 816.9 ± 4.5 Ma from an acidic volcanic rock of the Zhaertai Group in the Langshan Mts. and argued that the Zhaertai Group may represent an active rift basin of the Neo-Proterozoic. In the previous literatures, the boundary named Huogeqi Fault in tentative term between the Baoyintu and Zhaertai Groups was used to distinguish the NCC and CAOB (Fig. 1b) [18]. To the west of the Baoyintu Group in the Langshan Mts. outcrops a sedimentary sequence consisting of limestone with shale intercalations and quartz sandstone with blocks of limestone, termed as the Carboniferous Amushan Formation. Close to the China–Mongolia boundary area, are widely distributed the Ordovician Wubinaobao Formation consisting of slate with interlayers of siltstone and limestone and the Carboniferous–Permian Gaomiao Formation consisting of pyroclastic and clastic rocks [22].

In the study area, the Carboniferous–Permian granite-granodiorite intrusions of 320–259 Ma [19, 25–28] are widely distributed, and a few basic and intermediate intrusions such as the basic intrusions close to Baoyintu (328 ± 2 Ma, Han B. F. personal communication), the diorite intrusion at Langshan Reservoir (249 ± 5 Ma) [29]. Some monzogranite intrusions that are distributed in northeast trend closely in contact with the Baoyintu Group are dated to be 1,672 ± 10 Ma [20]. The Early Paleozoic intrusions include the quartz diorite (453 ± 5 Ma) along the China–Mongolia boundary area [7], and the muscovite plagiogranite intrusions at Huogeqi with a K–Ar age of ca. 412 Ma [19]. In addition, a few monzogranite intrusions are alleged to be Triassic [19] but lack of available age data.

Amphibolites with or without garnet occur as layers or lenses intercalated in metasedimentary rocks in the Baoyintu Group (Fig. 2a). Two representative garnet amphibolite samples were collected at N40°52′15.04″, E106°20′20.69″ (13LS02) and N40°52′17.45″, E106°20′44.85″ (13LS08) in Geeraobao Valley, southwest Langshan region.

3 Petrography and mineral compositions

The mineral compositions were determined using a JXA-8100 microprobe at Peking University. Operation conditions involved a 15-kV acceleration voltage, a 10-nA beam current, a 1–2 μm beam diameter, 15–20 s counting time and 5 s background counting times for each element (K^{α} for all measured elements). The K, Ca and Ti were measured by PETJ crystal, Na, Si, Mg and Al were analyzed by TAP crystal(s) (two separate channels), and Cr, Mn, Fe and Ni elements were analyzed by LIFH crystal. At final stage, PRZ correction is performed for all measured elements. Fifty-three kinds of natural and synthetic minerals of SPI Company were used for standardization. Representative mineral analyses are presented in Table 1.

The two studied samples are porphyroblastic with coarse garnet grains distributed in a matrix consisting mainly of preferably oriented amphibole and plagioclase (Fig. 2b). *Sample 13LS02* is composed of amphibole 50 vol%, quartz 20 %, garnet 15 %–20 %, plagioclase 5 %–10 %, with minor amount of rutile, titanite and ilmenite. The garnet porphyroblasts are up to 5–10 mm across. All the rutile grains are surrounded by ilmenite (Fig. 2c). *Sample 13LS08* consists of amphibole 63 vol%, quartz 13 %, plagioclase 11 %, garnet 8 %, chlorite 2 %, biotite 1 % with minor accessory phases of rutile, titanite and ilmenite. Garnet porphyroblasts are generally 0.6–1.8 mm across and show a typical "white-eye socket" or corona texture consisting of plagioclase and minor amount of amphibole, biotite and quartz (Fig. 2d, e). Some garnet grains contain inclusions of amphibole, titanite and quartz (Fig. 2e) or are highly fractured with amphibole and chlorite developing along the fractures (Fig. 2d). Garnet shows almandine content of 0.56–0.59, grossular of 0.26–0.28, pyrope of 0.11–0.13 and spessartine of 0.08–0.02, and minor zoning is observed with spessartine decreasing and pyrope increasing rimwards (Fig. 3). The highest pyrope content is measured at garnet rim (R1) when it contacts quartz (Figs. 2d, 3). Amphibole occurs as prismatic crystals in matrix, fine grains with plagioclase in corona and inclusions in garnet. The matrix amphibole (hb-1) is subhedral and yellow green or blue green with grain size of 0.3–1.5 mm (long axis). The amphibole as coronae (hb-2) is subhedral to anhedral with grain size of 0.1–0.3 mm, and the amphibole as inclusions (hb-0) is anhedral with grain size less than 0.1 mm. The three types of amphibole show similar compositions with Ca (M4) = 1.74–1.83, (Na + K) A = 0.20–0.37, Si = 6.30–6.76, Mg# = 0.43–0.59, TiO_2 = 0.1–0.77, being tschermakite, ferro-tschermakite and magnesio-hornblende according to Leake et al. [30]. However, they have different Al (M2) contents of 0.53–0.57 for hb-1, 0.37–0.48 for hb-2 and 0.43–0.48 for hb-0. Plagioclase occurs as anhedral to subhedral elongate grains with grain size of 0.2–1.2 mm (long axis) in matrix (pl-1) and as anhedral grains is 0.1–0.2 mm across in coronae around garnet (pl-2). Plagioclase of pl-1 shows lower anorthite (An) contents

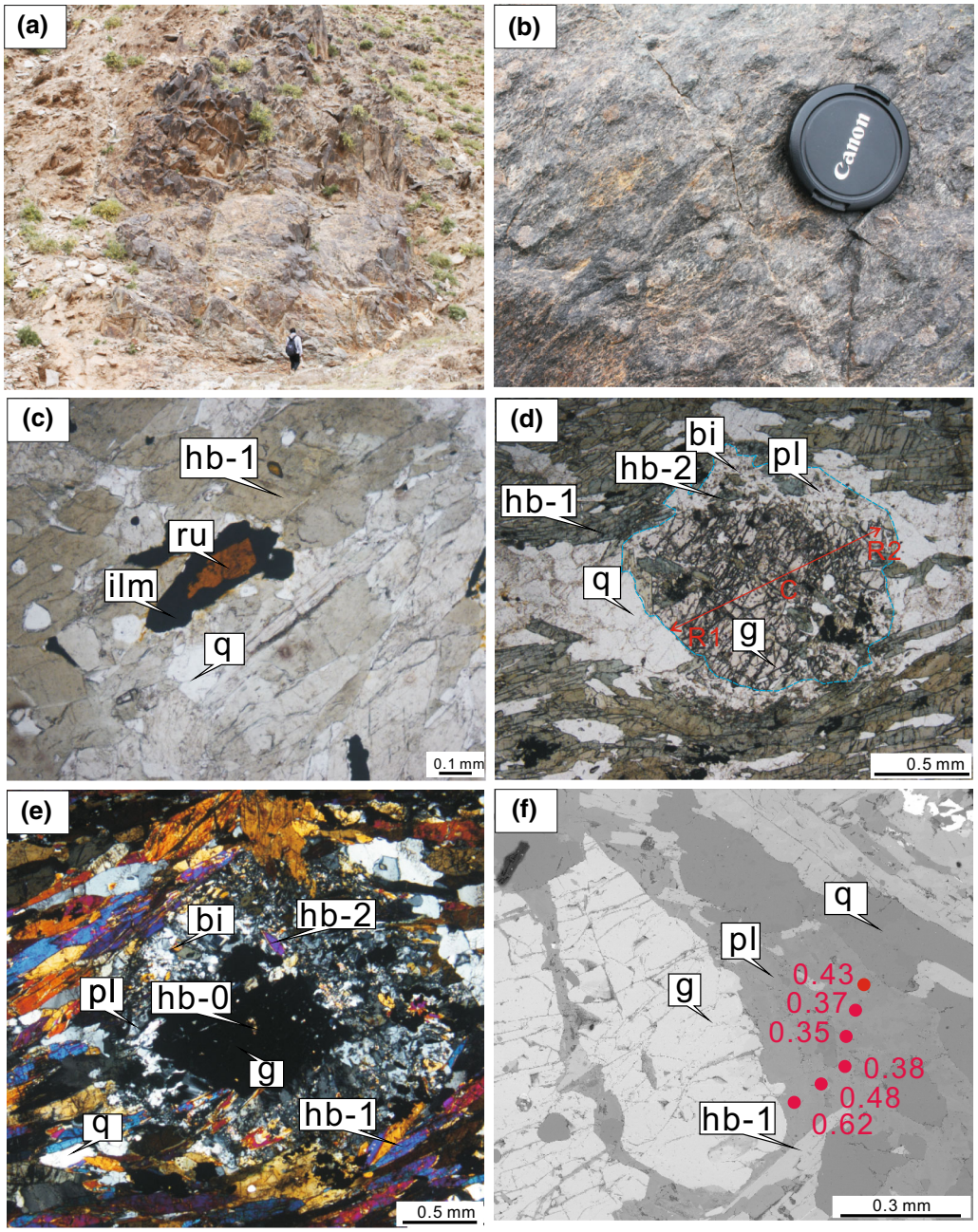

Fig. 2 (Color online) Field and petrographic characteristics of garnet amphibolites of the Baoyintu Group. **a** A garnet amphibolite lenticular block in mica schists. **b** Garnet porphyroblasts in a foliated matrix. **c** Photomicrograph displaying a rutile grain surrounded by ilmenite, sample 13LS02. **d** Photomicrograph displaying a garnet porphyroblast with an incomplete corona (upper margin of the grain) and numerous fractures, sample 13LS08. **e** Photomicrograph displaying a garnet grain with a wide corona and inclusions of amphibole, sample 13LS08. **f** Backscattered electron image displaying plagioclase composition zoning with An content in sample 13LS08. Mineral abbreviations: bi, biotite; chl, chlorite; g, garnet; hb, hornblende; ilm, ilmenite; pl, plagioclase; q, quartz; ru, rutile

(0.35–0.43) and generally has zoning with An increasing from core to rim, and pl-2 shows higher An contents of 0.38–0.62 (Fig. 2f). Biotite occurs as coronae around garnet and has $X_{Mg} = 0.51–0.53$ and $TiO_2 = 1.61$. Accessory minerals are dominated by ilmenite and titanite. A minor amount of rutile is commonly surrounded by ilmenite. Titanite occurs mainly as fine grains in matrix.

The textural relations and mineral compositions presented above suggest two main generations of mineral assemblages. Generation I involves garnet, hb-1

Table 1 Selected microprobe analyses for sample 13LS08

Sample	g-R1	g-C	pl-1C	pl-1R	pl-2	hb-0	hb-1	hb-2	bi	chl
SiO_2	37.62	37.78	59.10	56.33	52.33	45.28	42.19	43.62	36.06	24.95
TiO_2	0.00	0.07	0.00	0.00	0.01	0.26	0.10	0.35	1.61	0.07
Al_2O_3	21.18	20.74	25.97	26.82	29.53	12.33	16.04	14.38	17.65	20.81
Cr_2O_3	0.04	0.05	0.02	0.06	0.06	0.06	0.09	0.00	0.19	0.09
FeO	27.49	26.46	0.00	0.23	0.18	16.45	18.50	17.79	18.35	29.08
MnO	0.90	2.48	0.00	0.00	0.00	0.19	0.26	0.28	0.18	0.36
MgO	3.37	2.75	0.00	0.02	0.00	9.55	6.89	8.37	10.74	11.72
CaO	9.13	9.90	7.32	8.95	12.6	11.30	11.10	11.26	0.03	0.02
Na_2O	0.00	0.00	7.75	6.49	4.30	0.97	1.20	1.25	0.04	0.01
K_2O	0.00	0.00	0.03	0.05	0.03	0.38	0.64	0.43	9.79	0.01
Totals	99.73	100.23	100.19	98.95	99.04	96.77	97.01	97.73	94.64	87.12
O	12	12	8	8	8	23	23	23	11	14
Si	2.98	2.99	2.63	2.56	2.39	6.71	6.33	6.46	2.76	2.71
Ti	0.00	0.00	0.00	0.00	0.00	0.03	0.01	0.04	0.09	0.01
Al	1.97	1.93	1.36	1.43	1.59	2.16	2.84	2.51	1.59	2.66
Cr	0.00	0.00	0.00	0.00	0.00	0.01	0.01	0.00	0.01	0.01
Fe^{3+}	0.08	0.09	0.00	0.01	0.01	0.27	0.28	0.31	0.00	0.00
Fe^{2+}	1.74	1.66	0.00	0.00	0.00	1.78	2.04	1.89	1.17	2.64
Mn	0.06	0.17	0.00	0.00	0.00	0.02	0.03	0.04	0.01	0.03
Mg	0.40	0.32	0.00	0.00	0.00	2.11	1.54	1.85	1.22	1.90
Ca	0.77	0.84	0.35	0.44	0.62	1.80	1.78	1.79	0.00	0.00
Na	0.00	0.00	0.67	0.57	0.38	0.28	0.35	0.36	0.01	0.00
K	0.00	0.00	0.00	0.00	0.00	0.07	0.12	0.08	0.96	0.00
Total	8.00	8.00	5.02	5.01	5.00	15.31	15.43	15.42	7.83	9.95
X_{phase}	0.13	0.11	–	–	–	0.54	0.43	0.49	0.51	0.42
Y_{phase}	0.26	0.28	0.35	0.43	0.62	0.44	0.58	0.48	–	–

$X(g) = Mg/(Fe^{2+}+Mg + Ca + Mn)$, $X(hb) = Mg/(Fe^{2+}+Mg)$, $X(bi) = Mg/(Fe^{2+}+Mg)$, $X(chl) = Mg/(Fe^{2+}+Mg)$, $Y(g) = Ca/(Fe^{2+}+Mg + Ca + Mn)$, $Y(pl) = An = Ca/(Na + Ca)$, $Y(hb) = Al(M2)$. The mineral formulae were calculated with the program AX (Holland; http://www.esc.cam.ac.uk/astaff/holland/ax.html)

C core, *R* rim

amphibole, pl-1 plagioclase, rutile and quartz, and generation II consists of the corona assemblages involving hb-2 amphibole, pl-2 plagioclase, biotite, titanite, ilmenite and quartz. The inclusion assemblages in garnet may suggest an early stage of metamorphism.

4 Phase equilibria modeling and *P–T* path

For the mineral assemblages and compositions presented above, the model system MnNCKFMASHTO (Fe_2O_3) is chosen here to calculate *P–T* pseudosections for sample 13LS08. Quartz is considered to be in excess. A fluid phase is assumed to be pure H_2O and in excess for the subsolidus conditions, and a melt phase assumed to be in excess for the suprasolidus conditions.

The bulk-rock compositions obtained by ICP-OES analysis at China University of Geosciences (Beijing) for sample 13LS08 show $SiO_2 = 48.59$ (wt%), $TiO_2 = 2.12$, $Al_2O_3 = 15.10$, $TFe_2O_3 = 11.23$, $MnO = 0.18$, $MgO = 6.68$, $CaO = 9.89$, $Na_2O = 1.55$, $K_2O = 0.57$, $P_2O_5 = 0.82$ and $H_2O = 0.93$. The values were normalized in the MnNCKFMASHTO system where the O value is calculated by adding up the Fe^{3+} content calculated on the basis of charge and mass balance for each constituent mineral. The MnO in amphibole is neglected due to the lack of mixing models for Mn-bearing amphiboles. P_2O_5 is considered to be mainly present in apatite. The normalized results in the model system are $SiO_2 = 53.06$ (mol%), $TiO_2 = 1.74$, $Al_2O_3 = 9.72$, $FeO = 11.23$, $MnO = 0.11$, $MgO = 10.88$, $CaO = 11.91$, $Na_2O = 1.65$, $K_2O = 0.40$, $H_2O = 5.05$ and $O = 0.82$.

Calculations were performed using THERMOCALC 3.33, using the October 2009 updated version of the Holland & Powell [31] data set (tcds55.txt). Activity–composition relationships are those presented for garnet [32],

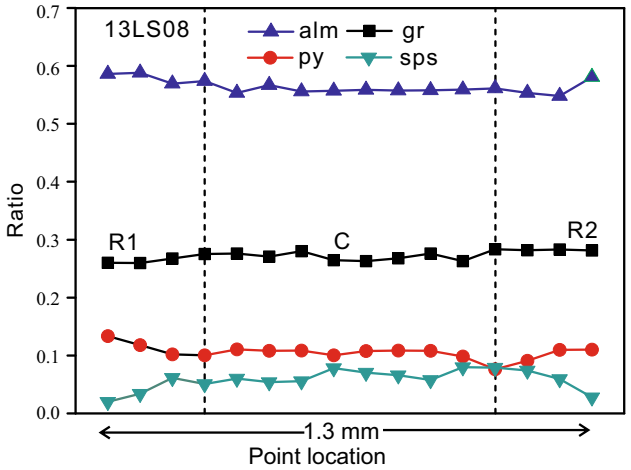

Fig. 3 (Color online) Zoning profiles of almandine (alm = Fe^{2+}/(Fe^{2+} + Mn + Mg + Ca)), grossular (gr), pyrope (py) and spessartine (sps) defined accordingly across a garnet grain in sample 13LS08. Labels C and R1 correspond to those in Table 1

clinopyroxene, glaucophane, cummingtonite and hornblende [33], plagioclase [34], chlorite [35], epidote [36], biotite and ilmenite [32]. The mixing model of melt [32] is used with a revision of deleting the "silL". Quartz, titanite and rutile are pure end-member phases.

A calculated MnNCKFMASHTO *P–T* pseudosection for sample 13LS08 is presented in Fig. 4. The observed two generations of mineral assemblage cannot match any predicted assemblages in the pseudosection. Contours of garnet compositions in Fig. 4 show that pyrope content in garnet increases mainly as temperature rises, and grossular content increases with the rising pressure until 1.2 GPa, but drops afterwards with further increase in pressure. Plotting of the pyrope and grossular contents for the measured values defines a *P–T* range of 710–740 °C/0.6–0.7 GPa in the assemblage g–hb–pl–bi–di–ilm–H_2O (or liq). Contours of An contents in plagioclase show that they mainly decrease as pressure rises under pressures above 0.6 GPa. The measured An content of 0.35–0.43 in pl-1 plagioclase indicates a pressure range from 1.3 to 1.1 GPa if assuming a fixed temperature of 725 °C, and the maximum An content of 0.62 measured in pl-2 plagioclase defines a pressure condition of 0.9 GPa for the fixed temperature. The zoning in pl-1 with increasing An from core to rim and the higher An contents in pl-2 suggests plagioclase growth with decreasing pressure. Contours of Al(M2) contents in amphibole indicate an increasing trend of the Al(M2) values with pressure rising. If assuming a fixed temperature of 725 °C, the measured Al(M2) contents for the three types of amphibole can yield pressures of 1.3–1.2 GPa for hb-1, 1.1–0.8 GPa for hb-2 and 1.1–0.9 GPa for hb-0. Thus, a decompression path can be inferred by plotting the mineral compositions in Fig. 4.

5 Geochronology

Sample 13LS02 was chosen for zircon U–Pb dating. Zircon grains were separated by conventional heavy liquid and magnetic separation followed by hand-picking under a binocular microscope. Selected grains were mounted in an epoxy resin, polished down to expose the grain center, photographed in transmitted and reflected light and imaged using cathodoluminescence (CL). The zircon LA-ICP-MS U–Pb isotopic analyses were performed at the Key Laboratory of Orogenic Belts and Crustal Evolution, Ministry of Education, Peking University. Zircon 91500 was used as the standard, and the standard silicate glass NIST was used to optimize the machine. The concentration of U, Th and Pb elements were calibrated using ^{29}Si as an internal calibrant and NIST 610 as an external reference standard. $^{207}Pb/^{206}Pb$, $^{206}Pb/^{238}U$ and $^{207}Pb/^{235}Pb$ ratios and apparent ages were calculated using the GLITTER 4.4 [37]. The age calculation and concordia plots were made using ISOPLOT [38] V4.45.

Zircon grains are rounded, with grain size 30–100 μm and length/width ratios of 1.0–1.5. They show sector or banded zoning in CL images (Fig. 5a), being of metamorphic origin. Twelve zircon grains were analyzed using LA-ICP-MS, and the results are presented in Table S1 and in Fig. 5b. All the analyses show Th/U = 0.01–0.04 and yield a concordant age of 399 ± 6 Ma with MSWD = 0.01.

6 Discussion and conclusions

6.1 Metamorphic *P–T* path and mineral evolution

Petrographic observation and phase modeling presented above suggest a decompression clockwise *P–T* path where the peak pressure condition can be constrained using the minimum An content in plagioclase and the Al(M2) content in hb-1 amphibole to be 1.2–1.3 GPa for the temperature conditions of 710–720 °C defined by garnet compositions. The other mineral compositions involving pl-1 and pl-2 plagioclase with higher An contents, hb-2 amphibole and garnet are modeled to indicate decompressional *P–T* conditions in pseudosections (Fig. 4), suggesting their post-peak growth and modifications. The obtained peak condition may correspond an assemblages g–hb–pl–bi–di–ep–ru–liq (+q), which is consistent with the presence of rutile, but the predicted diopside and epidote are not petrographically observed. Melt is also predicted to be present in the peak stage with a modal proportion of 4 % (mole on one oxide). This small amount of melt may be not well observed in petrography [39] or may be partly lost from the rock. However, if one-third of

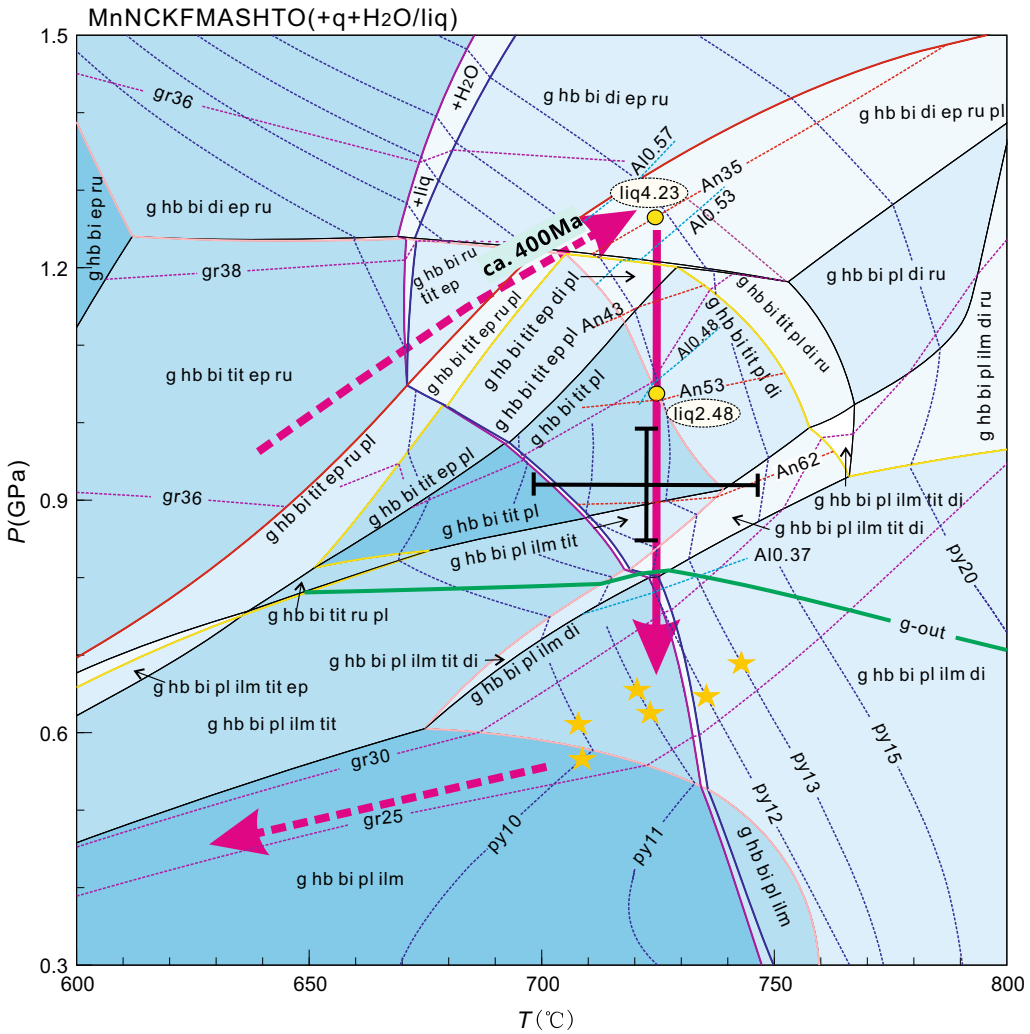

Fig. 4 (Color online) A *P–T* pseudosection for sample 13LS08 calculated in the system MnNCKFMASHTO with the excess of quartz, H_2O (the subsolidus fields) and liquid (the suprasolidus fields). The pseudosections are contoured with isopleths of pyrope (i.e., py15) and grossular (i.e., gr30) contents in garnet, the An content (i.e., An35) in plagioclase, the Al(M2) content (i.e., Al0.37) in amphibole. The yellow stars show the plotting of garnet compositions, and yellow dots show the calculated liquid content. The red dashed and solid arrows represent the inferred and constrained *P–T* path for the garnet amphibolite. The thick green line with "g-out" limits the garnet disappearance calculated in the NCKFMASHTO system without MnO using THERMOCALC. The dark black cross represents the *P–T* results calculated using the plagioclase–hornblende thermometer [40] and garnet–hornblende–plagioclase–quartz barometer [41]. The quini-variant fields are in white, and for the higher variant fields, the darker the color is shaded the higher the variance is. The mineral abbreviations are as follows: di, diopside; ep, epidote; liq, liquid; tit, titanite; other abbreviations are the same as in Fig. 2

the melt survives, it may trigger metamorphic reactions during decompression, i.e., g + di + ep + ru + -liq → hb + pl + tit/ilm, leading to rutile replaced by titanite at ~1.2 GPa, and subsequent disappearance of epidote and diopside at 1.0–1.1 GPa. The resultant assemblages may be g–hb–pl–bi–tit (+q), approximate to the observed mineral assemblage of generation I. The observed corona assemblage without garnet of generation II cannot be modeled in Fig. 4 because garnet may have been over stable due to Mn involvement in it but lack of available mixing models of Mn phases in other minerals. However, the temperature conditions of 710–740 °C defined by garnet compositions may be significant because as shown in Fig. 4 the pyrope contents were trivially affected by metamorphic reactions during an isothermal decompression. Thus, an alternative approach for constraining the peak conditions is to use the minimum An content in plagioclase and the maximum pyrope content in garnet rim. The isopleths of An = 0.35 and pyrope = 0.13 for sample 13LS08 give a *P–T* estimate of 1.25 GPa/725 °C with uncertainties of ~0.05 GPa and ~19 °C (one-sigma level) calculated using THERMOCALC.

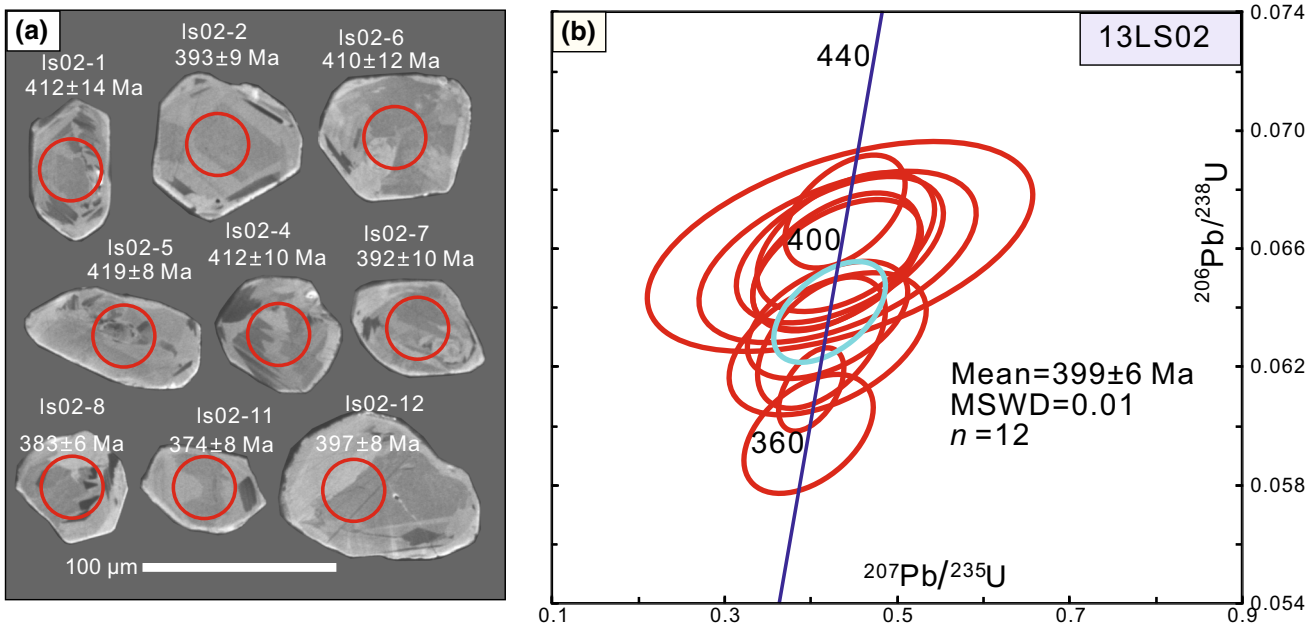

Fig. 5 (Color online) Cathodoluminescence (CL) photographs **a** and concordia diagram of zircon LA-ICP-MS U–Pb isotopic data **b** for sample 13LS02

Plagioclase is better than garnet for memorizing peak pressure conditions because diffusion of charge coupling species in plagioclase is always much slower than diffusion that involves similarly charged species such as Fe(Mg) and Ca in garnet [17]. As shown in Fig. 4, grossular contents in garnet could be largely modified during decompression, which defines a pressure estimate of ~0.6 GPa, slightly lower than the pressure defined by the minimum Al(M2) content in hb-2 amphibole. This suggests that garnet may have a tendency to get in equilibrium with the corona assemblage of generation II although it did belong to generation I in petrography.

The inclusion assemblages in garnet may indicate a prograde metamorphic stage prior to the peak stage, but the mineral compositions such as amphibole (hb-0), like their host garnet, may have been modified during decompression. The further metamorphic evolution after the isothermal decompression was inferred to be dominated by cooling with a slight decompression with a reference of the textural relations in the coexisting kyanite schists. Thus, a complete *P–T* path for sample 13LS08 is shown in Fig. 4.

For comparison, the *P–T* conditions for sample 13LS08 were further estimated by conventional thermobarometers. Using the hornblende–plagioclase thermometer [40] and the garnet–hornblende–plagioclase–quartz barometer [41], and choosing garnet compositions with the maximum pyrope, pl-1 plagioclase with the minimum An and hb-1 amphibole with maximum Al(M2) the *P–T* conditions were estimated to be 0.91 ± 0.08 GPa/722 ± 30 °C. Using the Ti-in-zircon thermometer [42], the temperatures were estimated mostly to be 646–694 °C where the activity of TiO_2 was assumed to be 0.6 for the common presence of ilmenite in the rock (Table S1). These temperatures are roughly consistent with the results given by garnet in pseudosections, and the pressure-estimate results are between the peak conditions defined by minimum An in pl-1 plagioclase and the decompression conditions defined by garnet and hb-2 amphibole.

6.2 Tectonic implications

The obtained zircon U–Pb age of 399 ± 6 Ma can be interpreted to represent the peak metamorphic stage or the prograde stages close to it. This interpretation can be supported from following lines of evidence: (1) the analyzed zircon grains show metamorphic origin from their CL images and Th/U values; (2) metamorphic evolution in the pre-peak stages are modeled to be dominated by dehydration and melting reactions, followed by melt crystallization during the early decompression stage, and the produced fluids or melt crystallization can facilitate zircon growth [43, 44]; and (3) the temperature estimates from Ti-in-zircon thermometer [42] suggest the zircon growth may occur during the prograde stages close to the peak.

Garnet amphibolite in the Baoyintu Group is recovered to experience a clockwise *P–T* path with the peak pressure stage corresponding to an apparent thermal gradient of 18 °C/km, being typical medium-pressure facies series [16]. Thus, the garnet amphibolite, together with the progressive metamorphic zones characteristic of appearances

of staurolite and kyanite in pelitic rocks in the Baoyintu Group, may suggest an orogenic event with crustal thickening [45]. We prefer to interpret this orogenic event at ca. 400 Ma to be a result of collision following the closure of the Paleo-Asian Ocean for there are a number of lines of evidence to support this view as proposed in articles [7–9, 15] although the other view that the Paleo-Asian Ocean may have lasted to Early Mesozoic [2–4, 6] seems more popular. This 400 Ma collision event is well consistent with the subduction event represented by the high-pressure and low-temperature metamorphism in the Ondor Sum Group with Ar–Ar ages of 446–453 Ma [14, 15].

The protoliths of the Baoyintu Group may represent a rifting basin of Meso-Proterozoic (<1,426 Ma) in the north periphery of the NCC [21]. As a member of North China Craton, it was involved in the collision and subjected to metamorphism as a result of the closure of the Paleo-Asian Ocean. From this point of view, the northern boundary of the North China Craton should be attributed to Tugurige Fault (Fig. 1b).

Acknowledgments This work was supported by the National Basic Research Program of China ("973" Program) (2013CB429801) and the China Survey of Geology (1212011121077). We sincerely thank Jiahui Qian, Renbiao Tao, Zhuang Li and Zhanzhan Duan for their valuable suggestions for preparing the manuscript. Hong Qin and Fang Ma are appreciated for their help in analyses of the bulk-rock compositions and LA-ICP-MS zircon U–Pb dating.

References

1. Sengör AMC, Natal'in BA, Burtman VS (1993) Evolution of the Altaid tectonic collage and Palaeozoic crustal growth in Eurasia. Nature 364:299–307
2. Xiao WJ, Windley B, Hao J et al (2003) Accretion leading to collision and the Permian Solonker suture, Inner Mongolia, China: termination of the Central Asian Orogenic Belt. Tectonics 22:1069–1089
3. Windley BF, Alexeiev D, Xiao WJ et al (2007) Tectonic models for accretion of the Central Asian Orogenic Belt. J Geol Soc (London) 164:31–47
4. Sengör AMC, Natal'in BA (1996) Paleotectonics of Asia: fragments of a synthesis. In: Yin A, Harrison TM (eds) The tectonic evolution of Asia. Cambridge University Press, Cambridge, pp 486–641
5. Chen B, Jahn BM, Wilde S et al (2000) Two contrasting Paleozoic magmatic belts in northern Inner Mongolia, China: petrogenesis and tectonic implications. Tectonophysics 328:157–182
6. Li JY, Gao LM, Sun GH et al (2007) Shuangjingzi middle Triassic syn-collisional crust-derived granite in the east Inner Mongolia and its constraint on the timing of collision between Siberian and Sino-Korean paleo-plates. Acta Petrol Sin 23:565–582 (in Chinese)
7. Xu B, Charvet J, Chen Y et al (2013) Middle Paleozoic convergent orogenic belts in western Inner Mongolia (China): framework, kinematics, geochronology and implications for tectonic evolution of the Central Asian Orogenic Belt. Gondwana Res 23:1342–1364
8. Tang KD (1990) Tectonic development of Paleozoic fold belts at the north margin of the Sino-Korean Craton. Tectonics 9:249–260 (in Chinese)
9. Shao JA (1991) Crust evolution in the middle part of the northern margin of Sino-Korean Plate. Peking University Press, Beijing, pp 1–135 (in Chinese)
10. Xu B, Chen B (1997) The orogenic tectonic and evolution in middle Paleozoic between North China Craton and Siberia Craton, in north Inner Mongolia. Sci Chin Ser D Earth Sci 27:227–232 (in Chinese)
11. Chu H, Zhang JR, Wei CJ et al (2013) A new interpretation of the tectonic setting and age of meta-basic volcanics in the Ondor Sum Group, Inner Mongolia. Chin Sci Bull 58:3580–3587
12. Zhang JR, Chu H, Wei CJ et al (2014) Geochemical Characteristics and tectonic significance of meta-basic volcanics in the Ondor Sum Group, Central Inner Mongolia. Acta Petrol Sin 30:1935–1947
13. Zhang JR, Wei CJ, Chu H (2014) Blueschist metamorphism and its tectonic implication of Late Paleozoic–Early Mesozoic metabasites in the mélange zones, central Inner Mongolia, China. J Asian Earth Sci 97:352–364
14. De JK, Xiao WJ, Windley BF et al (2006) Ordovician $^{40}Ar/^{39}Ar$ phengite ages from the blueschist-facies Ondor Sum subduction-accretion complex (Inner Mongolia) and implications for the Early Paleozoic history of continental blocks in China and adjacent areas. Am J Sci 306:799–845
15. Tang KD (1992) The tectonic evolution in the north fold belts of Sino-Korea Craton and its regularity of deposits formation. Peking University Press, Beijing, pp 1–264 (in Chinese)
16. Miyashiro A (1994) Metamorphic petrology. UCL Press Limited, London, p 404
17. Spear FS (1993) Metamorphic phase equilibria and pressure–temperature–time paths. Mineralogical Society of America, Washington, DC, p 799
18. Dong SB (1986) Metamorphism in China and its relation with crustal evolution. Geological Publishing House, Beijing, p 233 (in Chinese)
19. Exploration Institute of Geology and Mineral Resource of Inner Mongolia (2008) Tectonic construction map. China University of Geosciences Press, Wuhan (in Chinese)
20. Xu B, Liu SW, Wang CQ et al (2000) Sm–Nd, Rb–Sr geochronology of the Baoyintu Group in North western Inner Mongolia. Geol Rev 46:86–90 (in Chinese)
21. Sun LX, Zhao FQ, Wang HC et al (2013) Zircon U–Pb geochronology of meta-basic rocks from the Boyintu Block in the Langshan Area, Inner Mongolia, and its tectonic significance. Acta Geol Sin 87:197–207 (in Chinese)
22. Li WG (1996) The geology in Inner Mongolia autonomous region. China University of Geosciences Press, Wuhan, pp 197–203 (in Chinese)
23. Shen CL, Wang SG, Su XX et al (2004) Regional metallogenic characteristics in Proterozoic Group, Inner Mongolia. Earth Sci Front 11:279–286 (in Chinese)
24. Peng RM, Zhai YS, Wang JP et al (2010) Discovery of the Neoproterozoic acid volcanic rock in the south-western section of Langshan, Inner Mongolia. Chin Sci Bull 55:2611–2620 (in Chinese)
25. Hu HF, Zhang YQ, Hu HB et al (2013) Geochemical characteristics of Dishuigou diorite in Inner Mongolia and its geological significance. Geoscience 27:1308–1315 (in Chinese)
26. Wu YF, Zeng JN, Cao JJ et al (2013) Zircon U–Pb ages and Hf isotopes of Hercynian intrusion in Dongshengmiao, Inner Mongolia. Geol Sci Technol Inf 32:22–29 (in Chinese)
27. Yu YQ, Guo SY, Wang LF (2011) Characteristics and formation environment of Hercynian granites in Haorigeshan of Langshan, Inner Mongolia. Glob Geol 30:345–351 (in Chinese)

28. Pi QH, Liu CZ, Chen YL et al (2010) Formation epoch and genesis of intrusive rocks in Huogeqi ore field of Inner Mongolia and their relationship with copper mineralization. Miner Depos 29:437–451 (in Chinese)
29. Luo HL, Wu TR, Li Y (2007) Geochemistry and SHRIMP dating of the Kebu massif from Urad Zhongqi, Inner Mongolia: evidence for the Early Permian underplating beneath the North China Craton. Acta Petrol Sin 23:755–766 (in Chinese)
30. Leake BE, Woolley AR, Arpes CES et al (1997) Nomenclature of amphiboles: report of the Subcommittee on amphiboles of the International Mineralogical Association, Commission on New Minerals and Mineral Names. Am Miner 82:1019–1037
31. Powell R, Holland T, Worley B (1998) Calculating phase diagrams involving solid solutions via non-linear equations, with examples using THERMOCALC. J Metamorph Geol 16:577–588
32. White RW, Powell R, Holland TJB (2007) Progress relating to calculation of partial melting equilibria for metapelites. J Metamorph Geol 25:511–527
33. Diener JFA, Powell R (2012) Revised activity-composition models for clinopyroxene and amphibole. J Metamorph Geol 30:131–142
34. Holland TJB, Powell R (2003) Activity-composition relations for phases in petrological calculations: an asymmetric multicomponent formulation. Contrib Mineral Petrol 145:492–501
35. Holland TJB, Baker JM, Powell R (1998) Mixing properties and Activity-composition relationships of chlorites in the system $MgO–FeO–Al_2O_3–SiO_2–H_2O$. Eur J Mineral 10:395–406
36. Holland TJB, Powell R (1998) An internally consistent thermodynamic data set for phases of petrological interest. J Metamorph Geol 16:309–343
37. Anderson T (2002) Correction of common lead in U–Pb analyses that do not report ^{204}Pb. Chem Geol 192:59–79
38. Ludwig KR (2012) Isoplot/Ex Version 4.45: A geological toolkit for Microsoft Excel. Berkeley Geochronology Center Spec Publ, pp 1–70
39. White RW, Powell R, Holland TJB (2001) Calculation of partial melting equilibria in the system $Na_2O–CaO–K_2O–FeO–MgO–Al_2O_3–SiO_2–H_2O$ (NCKFMASH). J Metamorph Geol 19:139–153
40. Holland T, Blundy J (1994) Non-ideal interactions in calcic amphiboles and their bearing on amphibole–plagioclase thermometry. Contrib Mineral Petrol 116:433–447
41. Dale J, Holland T, Powell R (2000) Hornblende–garnet–plagioclase thermobarometry: a natural assemblage calibration of the thermodynamics of hornblende. Contrib Mineral Petrol 140:353–362
42. Ferry JM, Watson EB (2007) New thermodynamic models and revised calibrations for the Ti-in-zircon and Zr-in-rutile thermometers. Contrib Mineral Petrol 154:429–437
43. Roberts MP, Finger F (1997) Do U–Pb zircon ages from granulites reflect peak metamorphic conditions? Geology 25:319–322
44. Kelsey DE, Powell R (2011) Progress in linking accessory mineral growth and breakdown to major mineral evolution in metamorphic rocks: a thermodynamic approach in the $Na_2O–CaO–K_2O–FeO–MgO–Al_2O_3–SiO_2–H_2O–TiO_2–ZrO_2$ system. J Metamorph Geol 29:151–166
45. England PC, Thompson AB (1984) Pressure–temperature–time paths of regional metamorphism I. Heat transfer during the evolution of regions of thickened continental crust. J Petrol 25:894–928